SCIENCE CHINA
Information Sciences

• LETTER •

September 2026, Vol. 69, Iss. 9, 199402:1–199402:2
https://doi.org/10.1007/s11432-025-4806-3

# A ScAlN thin-film-based piezoelectric fused silica ring gyroscope exhibiting 0.45°/h bias instability

Ronghui FENG[1], Zheng LI[1], Shuiyang LIANG[2,3], Qingsong LI[2,3], Sheng LIU[1*], Dingbang XIAO[2,3*] & Guoqiang WU[1*]

[1]*School of Integrated Circuits, Wuhan University, Wuhan 430072, China*
[2]*College of Intelligence Science and Technology, National University of Defense Technology, Changsha 410073, China*
[3]*National Key Laboratory of Equipment State Sensing and Smart Support, National University of Defense Technology, Changsha 410073, China*

Received 28 November 2025/Revised 22 January 2026/Accepted 13 February 2026/Published online 12 August 2026

**Citation** Feng R H, Li Z, Liang S Y, et al. A ScAlN thin-film-based piezoelectric fused silica ring gyroscope exhibiting 0.45°/h bias instability. Sci China Inf Sci, 2026, 69(9): 199402, https://doi.org/10.1007/s11432-025-4806-3

Thin-film piezoelectric microelectromechanical system (MEMS) gyroscopes have attracted considerable research interest recently, propelled by progress in piezoelectric thin-film fabrication technologies and their inherent advantages such as high electromechanical efficiency, wide linearity, and elimination of DC bias or narrow structural gaps, relative to their electrostatic counterparts. To date, the majority of these gyroscopes are constructed on a thin-film piezoelectric-on-single-crystal silicon (SCS) platform, wherein SCS acts as the primary vibrating structure [1]. Nevertheless, the reported SCS-based piezoelectric MEMS gyroscopes suffer from limited quality factors ($Q$) [2,3], mainly due to the constraints imposed by the large coefficient of thermal expansion (CTE) and inherent anisotropy of SCS. Consequently, their bias instability (BI) performance is inferior to that of capacitive MEMS gyroscopes.

Recent studies on fused silica-based MEMS gyroscopes have demonstrated high-$Q$ [4], enabled by the isotropic material properties and low CTE of fused silica, which positions fused silica as a promising material for developing high-$Q$ piezoelectric MEMS gyroscopes. To the best of the authors' knowledge, this study reports the first scandium aluminum nitride (ScAlN) thin-film-based piezoelectric fused silica MEMS ring gyroscope, which simultaneously achieves an ultra-high $Q$ and, consequently, exceptional BI performance. This work thus offers valuable insights for advancing the development of high-performance piezoelectric MEMS gyroscopes.

*Device design.* The designed silica MEMS ring gyroscope comprises a supportive substrate, a device body, and piezoelectric functional stacks, which are arranged sequentially from bottom to top (Figure 1(a)). The ring gyroscope is suspended above a cavity in the substrate via eight folded support tethers. The top electrode of the piezoelectric ring gyroscope is uniformly divided into eight segments. Each segment is further split into inner and outer subparts, with all parts electrically isolated. This electrode configuration is designed to match the stress distribution of the operating mode. To eliminate thermal mismatch, both the substrate and the device body are fabricated from fused silica. Additionally, several fused silica mass blocks are distributed around the ring to facilitate laser trimming, thereby enabling precise mode matching.

*Operational principles.* The designed ring gyroscope operates in a deliberately chosen in-plane wineglass mode ($n = 2$), which preserves modal symmetry and degeneracy and naturally exploits the $d_{31}$ piezoelectric coupling of the ScAlN thin film. Figure 1(b) illustrates the stress distribution on the top surface of the piezoelectric thin film during device operation. When phase-opposed voltages are applied to the electrode pairs aligned along the anti-node axis of the primary mode, counteracting stress fields (compressive versus tensile) are generated, which in turn excite the primary mode. Rotation perpendicular to the ring plane ($z$-axis) induces Coriolis force coupling, which hence excites the secondary mode. This excitation leads to strain-dependent charge accumulation, which can be detected at the orthogonal electrode pairs, specifically, those located on the anti-node axis segments of the secondary mode.

*Fabrication.* The reported piezoelectric MEMS ring gyroscope is fabricated on a thin-film piezoelectric-on-fused-silica platform, as depicted in Figure 1(c). Piezoelectric stacks with a layered structure of molybdenum (Mo)-ScAlN-titanium-tungsten (TiW)/gold (Au) with thicknesses of 0.2 μm-1 μm-0.1 μm/0.4 μm are deposited sequentially onto a 500-μm-thick fused silica wafer, a thickness chosen to balance fabrication requirements with adequate modal separation for stable operation. The ScAlN and gold layers are patterned separately. The ScAlN layer is patterned to enable access to the underlying Mo electrode, while the gold layer is patterned to form the top electrodes. Additionally, an oxide thin film is deposited and patterned, which not only prevents potential electrical shorting between the top and bottom electrodes but also acts as a passivation layer for the top electrodes.

Subsequently, the gyroscope structures are patterned and released using femtosecond laser assisted etching (FLAE) technology [4]. In this process, the ring, mass blocks, and support tethers are first patterned via femtosecond laser modification, followed by backside structural release via 1.5-hour wet etching in a 10 vol% hydrofluoric acid solution, with the front side protected by a pho-

* Corresponding author (email: shengliu@whu.edu.cn, dingbangxiao@nudt.edu.cn, wuguoqiang@whu.edu.cn)

 

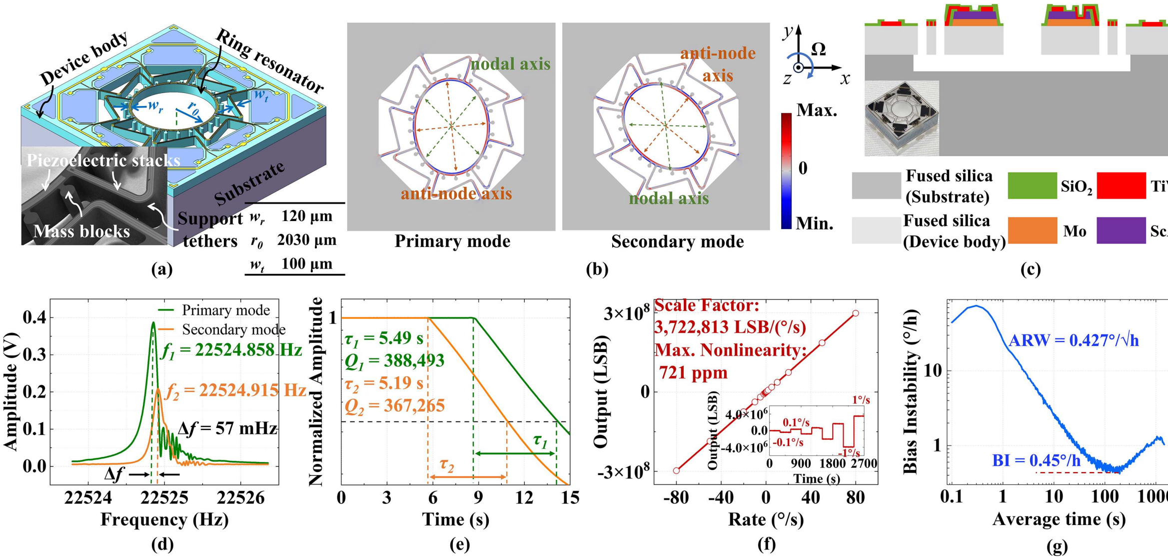


**Figure 1** (Color online) Design and measurement results of the reported piezoelectric fused silica ring gyroscope. (a) Schematic diagram and key dimensions of the gyroscope structure. Inset: Magnified SEM image showing a partial view of the ring, mass blocks, and support tethers. (b) Stress distribution on the top surface of the ScAlN thin film during device operation. Red represents tensile stress, and blue represents compressive stress. (c) Cross-sectional view of the fabrication platform. Inset: Optical image of the fully assembled ring gyroscope. (d) Amplitude-frequency response curves. (e) Ring-down curves of the primary and secondary modes. (f) Rotation rate response of the gyroscope in rate mode. Inset: Time-domain response during rotation at ±0.1°/s to ±1°/s over a 2700 s duration. (g) Allan deviation plot for characterizing the gyroscopes' stability.

toresist layer. The etch selectivity between the laser-modified and unmodified fused silica regions is approximately 10:1, which translates to a final device thickness of 498.5 μm. Following structural release, the fully freestanding device is bonded via a conductive adhesive (JM7000) to a supporting substrate featuring a pre-etched cavity (inset of Figure 1(c)). A magnified scanning electron microscopy (SEM) image of the fabricated gyroscope is provided in the inset of Figure 1(a), in which the ring structure, top electrodes, mass blocks, and support tethers are clearly distinguishable.

*Experimental investigation.* The fabricated ring gyroscope is die-attached and wire-bonded to a customized ceramic carrier. Subsequently, laser trimming is performed to reduce the frequency split between degenerate modes and achieve effective mode matching. Following laser trimming, the gyroscope is vacuum-encapsulated at the chip scale with an integrated getter to maintain a pressure below 1 Pa, thereby suppressing gas damping. The packaged device is then characterized using a Zurich Instruments MFLI lock-in amplifier. The measured amplitude-frequency responses and ring-down curves for the primary and secondary modes are illustrated in Figures 1(d) and (e), respectively. For the degenerate modes, the measured frequencies are 22524.858 and 22524.915 Hz, resulting in a frequency split of approximately 57 mHz. Additionally, analysis of the ring-down curves yielded $Q$s of 388493 and 367265 for the primary and secondary modes, respectively, benefiting from the symmetric in-plane mode design, the intrinsically low mechanical loss of fused silica, as well as the low-loss support tether architecture.

Device performance is characterized via a closed-loop force-to-rebalance scheme, employing FPGA-based control with 32-bit processing and a 16-bit DAC. The drive-mode vibration amplitude is maintained at approximately 0.5 μm. The rotation rate response, measured across a range of ±0.1°/s to ±80°/s, is presented in Figure 1(f). The inset displays the time-domain response during rotation at ±0.1°/s to ±1°/s over a 2700 s duration. Key performance metrics comprise a digital scale factor of $3.722813\times10^6$ LSB/(°/s), with a corresponding physical counterpart of 4.072 mV/(°/s), enabled by high mechanical gain from the small frequency split and high $Q$, and a maximum nonlinearity of 721 ppm. As depicted in Figure 1(g), Allan deviation analysis yields an angle random walk (ARW) of $0.427°/\sqrt{\mathrm{h}}$ and a BI of 0.45°/h. The theoretical thermal noise limit is approximately $0.00181°/\sqrt{\mathrm{h}}$.

In comparison to state-of-the-art piezoelectric MEMS gyroscopes [2, 3, 5], the present work achieves an order-of-magnitude higher $Q$ and demonstrates the first BI breakthrough below 1°/h for this class of devices. This translates to an order-of-magnitude improvement in the BI metric, thereby highlighting the significant potential of fused silica-based architectures for advancing high-performance piezoelectric MEMS gyroscopes.

**Acknowledgements** This work was supported in part by National Natural Science Foundation of China (Grant No. 62322409), and Fundamental Research Funds for the Central Universities (Grant No. 2042025kf0028).

## References


1 Yang S, Wu Z, Jia W, et al. Ultra-low relative frequency split piezoelectric ring resonator designed for high-performance mode-matching gyroscope. J Microelectromech Syst, 2022, 31: 6–8
2 Qi Z, Wang B, Zhai Z, et al. Bridging piezoelectric and electrostatic effects: a novel piezo-MEMS pitch/roll gyroscope with sub 10°/h bias instability. Microsyst Nanoeng, 2024, 10: 160
3 Liu Z, Wen H, Ayazi F. Multi-coefficient eigenmode operation-breaking through 10°/h open-loop bias instability in wideband aluminum nitride piezoelectric BAW gyroscopes. Microsyst Nanoeng, 2023, 9: 18
4 Wang C, Wu K, Wang X, et al. A MEMS disk gyroscope with high fabrication precision, high quality factor (>810k) and high overload characteristic (>15000 g). J Phys-Conf Ser, 2024, 2740: 012062
5 Ontronen A, Kaajakari V, Ishii M, et al. A PiezoMEMS lissajous frequency-modulated gyroscope: stability, vibration robustness, and challenges. IEEE Sens J, 2024, 24: 34170–34178